Size-Templating Matrix Effect in Vesicle Formation. 2. Analysis of a Macroscopic Model

ARTICLE *in* THE JOURNAL OF PHYSICAL CHEMISTRY B · NOVEMBER 2003

Impact Factor: 3.3 · DOI: 10.1021/jp034590+

Size-Templating Matrix Effect in Vesicle Formation. 2. Analysis of a Macroscopic Model

C. D. Bolton[†] and J. A. D. Wattis*[,†]

Theoretical Mechanics, School of Mathematical Sciences, University of Nottingham, University Park, Nottingham, NG7 2RD, U.K.

Received: March 7, 2003

Recently it has been reported that the growth of vesicles is strongly influenced by the presence of pre-added vesicles. In particular, the size distribution of vesicles is sharply centered about the size of the pre-added vesicles: the size-templating "matrix" effect. A description of the dynamics of the concentrations of cluster sizes has been proposed Bolton and Wattis (*J. Phys. Chem. B* **2003**, *107*, 7126), in terms of a nonlinear microscopic model that is valid far from equilibrium while agreeing with the equilibrium cluster size distribution data. In this paper we approximate this model by a coarse-graining reduction to a low-dimensional dynamical system, a process introducing two parameters on which the solution depends. We solve the system in two parameter regimes and demonstrate that there is a borderline case between the two types of solution that contain features of each. In each case matched asymptotics are used to derive the solution over a series of time scales, and we consider a range of initial conditions including experimentally relevant cases where a small concentration of vesicles is pre-added. We interpret these results on a phase-plane diagram to illustrate how the matrix effect manifests itself in this model.

1. Introduction

Self-reproducing molecular systems have been widely investigated[1,4−6,8−10] because they exhibit the fundamental properties of a living system and have the potential to model life evolving in pre-biotic conditions. One such self-reproducing system recently receiving attention is that of vesicles, which are constructed from individual surfactant molecules, particularly POPC/oleate. If the concentration of individual surfactant molecules (monomer) exceeds the critical aggregate concentration (CAC), then vesicles spontaneously form, driven by an increase in the entropy of the surrounding water. The structure of the vesicle, a spherical lipid bilayer with an aqueous core separated from the surrounding environment, has a tantalizing analogy with a biological cell.[1] Experimental results have demonstrated that an autocatalytic process is involved with the growth of vesicles. We have proposed a microscopic model of vesicle growth[2] based on a novel generalization of the Becker−Döring model of nucleation[3] and confirmed its validity with numerical simulations. In this paper we reduce the microscopic model to a low-dimensional system of equations and solve this using matched asymptotic analysis.

The experiments we aim to model have been conducted by Luisi's group at ETH.[4−6,8−10] Walde et al.[4] used fatty acid (caprilic and oleic) vesicles to demonstrate an autopoietic self-reproductive process, that is, an increase in the formation of vesicles due to a reaction within the boundary of existing vesicles. Such an autocatalytic effect was confirmed by Blöchliger et al.[5] who demonstrated that the phase lag is much reduced by the presence of pre-added vesicles, by comparing a system that initially consists of only monomers to a system that, in addition, initially has some vesicles present. These experiments relied on the hydrolysis of a precursor to produce the monomeric surfactant required to construct the vesicles, and the catalytic nature arises from the fact that the vesicles themselves efficiently hydrolyze the precursor. Mavelli and Luisi[6] proposed a simplified kinetic model of this system and later Coveney and Wattis[7] formulated, and studied, a nonlinear mathematical model of the formation of vesicles from a precursor. Recent experiments have been initiated from a stock of surfactant, eliminating the reliance on the hydrolysis of a precursor.

These later experiments have highlighted a second process, whereby vesicles catalyze the aggregation of monomers into vesicles. Blöchliger et al.[5] investigated the growth of oleic acid/oleate vesicles by pre-adding vesicles with a monodisperse distribution (with mean size either 50 or 100 nm) to an initial stock of surfactant. By "monodisperse" vesicles we mean a distribution of vesicle sizes centered about a particular size with a very small standard deviation. The growth of vesicles was observed by a combination of freeze fracture electron microscopy and turbidity measurements. The final distribution of vesicle size was found to be strongly biased toward the diameter of the pre-added vesicles: this phenomenon was labeled the "matrix" effect. In contrast, without any pre-added vesicles, the final distribution was relatively polydisperse. Further work by Lonchin et al.[8] demonstrate the matrix effect for a system of oleate micelles with pre-added POPC (1-palmitoyl-2-oleate-*sn*-glycero-3-phosphocholine) vesicles and claim their results are applicable to a wide range of vesicular systems. For a system with pre-added vesicles the kinetics are separated into at least two phases, first a fast phase over which the pre-added vesicles are templated; this is followed by a very slow phase of virtual inactivity. In contrast, a system without pre-added vesicles has slower, but more sustained, dynamics.

A drawback of the above experiments is that it is impossible to distinguish in the final distribution between the contribution from pre-added, or newly formed, vesicles. To overcome this, a novel experiment was pioneered by Berclaz et al.[9] where the pre-added vesicles were "tagged" by trapping ferritin molecules inside the vesicle; due to the dense iron core of the ferritin molecule, these can easily be detected by cryotransmission electron microscopy analysis. It was concluded that the initial

[†] E-mail addresses: colin.bolton@maths.nottingham.ac.uk, Jonathan.Wattis@nottingham.ac.uk.

* Corresponding author.

10.1021/jp034590+ CCC: $25.00
Published on Web 11/26/2003

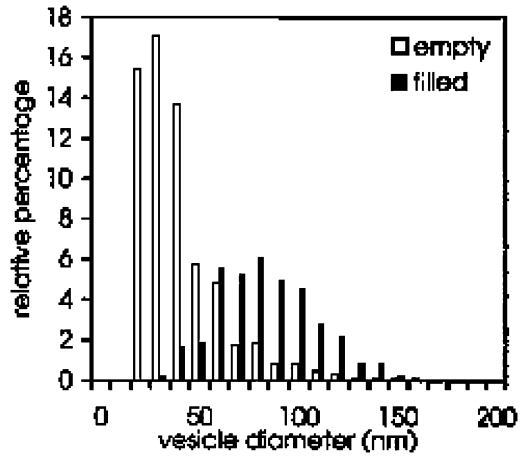

Figure 1. Pre-added vesicles were tagged with ferritin molecules and added to a stock of monomeric surfactant. We reproduce the plot of the number weighted distribution for filled and empty vesicles in the final size distribution. Clearly the empty vesicles are predominantly smaller than the filled vesicles. Printed with permission of P. L. Luisi.

monomers were mostly concentrated in new vesicles with a size that does not exceed the size of the pre-added vesicles; see Figure 1. Berclaz et al.[9,10] exploited this technique to investigate the mechanism of vesicle growth in the presence of pre-added vesicles for oleic acid/oleate and POPC/oleic acid/oleate vesicles. If the "matrix" effect is to be explained by an accelerated de novo vesicle formation, we would expect the new vesicles to be untagged by ferritin molecules contained in the pre-added vesicles. Alternatively, we envisage a new process of vesicle formation, a monomer−cluster−cluster interaction, in the presence of a complete vesicle a secondary smaller vesicle or vesicle fragment can grow relatively rapidly (compared with de novo growth). There must also be a fission mechanism by which these disengage to form two vesicles. In such a scheme the ferritin molecules will be redistributed among all the vesicles during the fission process; hence in the final distribution we would expect to observe many tagged vesicles. In fact, the latter case was found to be prevalent, so it was concluded that not only did a fission process exist but also that it dominates the de novo process.

This introductory section concludes with a brief description of the Becker−Döring model of nucleation, and we present the microscopic model previously proposed for the growth of vesicles.[2] It was concluded that a theoretical analysis of this microscopic model was not possible due to its complexity and in section 2 we use a coarse-graining technique to approximate the problem by a low-dimensional system of equations. Once the system is established, we analyze it in section 3, using matched asymptotic expansions. The form of the solution depends on the choice of parameters in the coarse-graining procedure, and we investigate these in turn. Having solved the system, we interpret the results in terms of a phase-plane diagram in section 4; though this is still based on the low-dimensional approximation, it gives further insight into the dynamic behavior of the high-dimensional microscopic model. This paper concludes with a discussion of the results in section 5.

1.1. Becker−Döring Equations. The Becker−Döring equations were originally formulated to describe the kinetics of nonequilibrium gas−liquid transitions, where it was proposed that clusters form by the addition, or subtraction, of single particles (monomers) with no interaction between larger clusters. Such larger clusters evolve by maintaining a dynamic balance of monomer aggregation and fragmentation. This process is modeled as a chemical reaction, denoting an r-sized cluster as C_r, we have the reversible reaction

$$C_r + C_1 \rightleftharpoons C_{r+1} \tag{1.1}$$

We define $c_r(t)$ to be the concentration of clusters C_r at time t. For each reaction there are two reaction rates to prescribe; we denote the forward rate by a_r and the reverse by b_{r+1}, both nonnegative. In the original formulation, the concentration of monomers was assumed constant, later Penrose and Lebowitz[11] generalized this model to allow the monomer concentration to vary, instead ensuring the conservation of mass

$$\rho = \sum_{r=1}^{\infty} r c_r \tag{1.2}$$

This modified model is still referred to as the Becker−Döring model. The stepwise aggregation and fragmentation is the central feature of the Becker−Döring model and is an inherent assumption underlying all the following analysis. Defining J_r as the net flux from a cluster of size r to a cluster of size $r + 1$ we express the system by

$$\dot{c}_1 = -J_1 - \sum_{r=1}^{\infty} J_r \tag{1.3}$$

$$\dot{c}_r = J_{r-1} - J_r \qquad r \geq 2 \tag{1.4}$$

$$J_r = a_r c_1 c_r - b_{r+1} c_{r+1} \qquad r \geq 1 \tag{1.5}$$

We define Q_r, the cluster partition function, in terms of the forward, and reverse, reaction rates by $a_r Q_r = b_{r+1} Q_{r+1}$ and insist that $Q_1 = 1$; the system then has a unique equilibrium solution, denoted by $\bar{c}_r = Q_r \bar{c}_{1r}$. The quantity

$$V = \sum_{r=1}^{\infty} c_r \left(\log\left(\frac{c_r}{Q_r}\right) - 1 \right) \tag{1.6}$$

decreases monotonically with time and is also bounded below. It thus qualifies as a Lyapunov function and is associated with a free energy of the system.

1.2. Microscopic Model of Vesicle Formation. In a previous paper[2] we generalized the Becker−Döring model (1.3)−(1.5) to include a new mechanism. We proposed that an existing vesicle offers a catalytic surface on which a vesicle fragment can grow at an accelerated rate. We assumed that when the fragment grows to the same size as the host vesicle it disengages to result in two vesicles of equal size. The growth rate of the fragment was assumed to have the same size dependence as for de novo growth of a vesicle, but accelerated by a constant factor (γ). Finally, we assumed that while a fragment is growing, the host vesicle remains inert and any available monomers are captured by the fragment. Denoting $F_{r,k}$ to be a vesicle with r monomers harboring a fragment of k monomers, we have the following reactions in addition to (1.1)

$$C_r + C_1 \rightleftharpoons F_{r,1} \qquad (\delta_r, \delta_r/A) \tag{1.7}$$

$$F_{r,k} + C_1 \rightleftharpoons F_{r,k+1} \qquad (\alpha_{r,k}, \beta_{r,k+1}) \tag{1.8}$$

$$F_{r,r} \rightleftharpoons 2C_r \qquad (\phi_r, A\phi_r) \tag{1.9}$$

where the forward and reverse reaction rates are shown after each reaction. Reaction 1.7 combines a monomer with a cluster

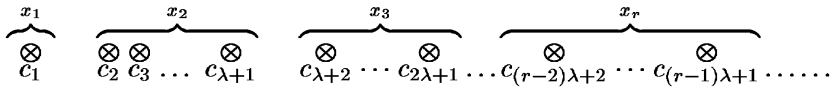

Figure 2. Diagram of a simple coarse-graining procedure where x_n represents the new coordinates and c_n the old concentrations. In this example the number of cluster sizes grouped together to form each x_n is λ, except for the monomer concentration, which is represented by x_1. In general, λ can be made nonuniform, i.e., $\lambda = \lambda_r$.

to form a vesicle with a monomer fragment, reaction 1.8 allows the fragments to grow, and reaction 1.9 permits the fragment to disengage the host vesicle when they are the same size. We assume $a_r = \epsilon$ ($\epsilon \ll 1$); hence $b_{r+1} = \epsilon Q_r/Q_{r+1}$ so that the correct equilibrium solution is approached, given by

$$\bar{c}_r = Q_r \bar{c}_1^r \qquad \bar{f}_{r,k} = AQ_rQ_k\bar{c}_1^{r+k} \tag{1.10}$$

where $f_{r,k}$ denotes the concentrations of $F_{r,k}$ fragment/host pairs. The partition function was chosen to have the form

$$Q_r = \exp(\Theta r^3 + \Pi r^2 + \Omega r - \Theta - \Pi - \Omega) \tag{1.11}$$

The parameter A arises from insisting on a detailed balancing condition at equilibrium, and to agree with experimental observations at late stages, we require $A \ll 1$; so few vesicle−vesicle combinations are observed. Modeling (1.1) and (1.7)−(1.9) using the law of mass action, and making some further assumptions on the size-dependence of the parameters, we previously obtained

$$\dot{c}_1 = -J_1 - \sum_{r=1}^{\infty} J_r - \sum_{r=2}^{\infty}\left(\delta c_r c_1 - \frac{\delta}{A} f_{r,1}\right) - \sum_{r=2}^{\infty}\sum_{k=1}^{r-1} H_{r,k} \tag{1.12}$$

$$\dot{c}_r = J_{r-1} - J_r + 2\phi f_{r,r} - 2A\phi c_r^{\,2} - \delta c_r c_1 + \frac{\delta}{A} f_{r,1} \qquad (r \le 2) \tag{1.13}$$

$$\dot{f}_{r,1} = \delta c_r c_1 - \frac{\delta}{A} f_{r,1} - H_{r,1} \tag{1.14}$$

$$\dot{f}_{r,k} = H_{r,k-1} - H_{r,k} \qquad (1 < k < r) \tag{1.15}$$

$$\dot{f}_{r,r} = H_{r,r-1} - \phi f_{r,r} + A\phi c_r^{\,2} \tag{1.16}$$

$$J_r = \epsilon\left(c_1 c_r - \frac{Q_r}{Q_{r+1}} c_{r+1}\right) \tag{1.17}$$

$$H_{r,k} = \epsilon\gamma\left(f_{r,k} c_1 - \frac{Q_k}{Q_{k+1}} f_{r,k+1}\right) \tag{1.18}$$

and we assume that $\epsilon\gamma \sim \mathcal{O}(1)$ so that the fragment growth far exceeds the growth of vesicles via mechanism (1.1). Previously we demonstrated the validity of this model by comparing numerical simulations with experimental results but no direct theoretical analysis was possible.

2. Coarse Graining

2.1. General Contraction. The drawback of a microscopically detailed model is that there is not only a vast number of equations to be solved but also a similar number of parameters to be determined. A coarse-graining procedure for the Becker−Döring model has already been discussed and successfully applied to micelle formation,[12] and a more detailed study of the renormalization procedure is given by Wattis and Coveney[15,16] and Bolton and Wattis.[13] In the present section we summarize this procedure and derive a low-dimensional system of equations that approximate the model of vesicle formation being considered in this paper, namely (1.12)−(1.18).

The basic idea behind the coarse-graining procedure is to use a mesh function to gather the concentrations into groups of consecutive sizes. Each group is then represented by the concentration of one particular cluster size in the group. The dynamics of these representative concentrations is governed by a set of coarse-grained equations based on the original equations. We note that throughout this process the monomer concentration is kept distinct due to its unique nature within the Becker−Döring scheme. To illustrate the method, we consider an example where the first λ cluster sizes, after the monomers, are grouped together. Each block of clusters to be grouped together thereafter also contains λ cluster sizes. That is, if $\lambda = 2$, then we group together c_2 and c_3 to form x_2, where x_1 has been reserved for the monomer concentration, c_4 and c_5 would then form x_3, etc. The larger the parameter λ, the greater the number of cluster sizes gathered in each group, the more coarse-grained the system is, and hence the less microscopic detail that is preserved. We picture this diagrammatically in Figure 2, where, in general, x_n represents concentrations from $c_{(n-2)\lambda+1}$ to $c_{(n-1)\lambda+1}$. In this scheme we have assumed that the number of cluster sizes being assigned to each x_n is the same, with the exception of x_1; however, the theory can easily be generalized to allow this to vary with aggregation number, n. For the time being we remain with the example where λ is independent of n. We systematically deduce a flux from x_n to x_{n+1}, L_n, by eliminating the concentrations $c_{(n-1)\lambda+2}$ to $c_{n\lambda}$ from the set of microscopic fluxes $J_{(n-1)\lambda+1}$, ..., $J_{n\lambda}$. Then we define $x_n = c_{(n-1)\lambda+1}$ and $x_{n+1} = c_{n\lambda+1}$; that is, we set the coarse-grained effective concentration to that of the largest cluster size in the group. This choice ensures that when $\lambda = 1$ the original system is recovered. Performing the elimination yields

$$L_n = \alpha_n x_n x_1^{\lambda} - \beta_{n+1} c_{n+1} \tag{2.1}$$

$$\alpha_n = T_n \prod_{p=1}^{\lambda} a_{(n-1)\lambda+p} \qquad \beta_{n+1} = T_n \prod_{p=2}^{\lambda+1} b_{(n-1)\lambda+p} \tag{2.2}$$

where T is found by matching the time scales and steady-state solutions between the original and coarse-grained systems.[13] In the aggregation term of the flux the monomer concentration is now raised to a power of λ, which reflects the fact that, on average, λ monomers are required to aggregate with a cluster to take it from x_n to x_{n+1}. The governing equations for the contracted concentrations are

$$\dot{x}_1 = -\lambda L_1 - \sum_{n=1}^{\infty} \lambda^2 L_n \tag{2.3}$$

$$\dot{x}_n = L_{n-1} - L_n \qquad \forall n \ge 2 \tag{2.4}$$

Bolton and Wattis[13] have shown that the coarse-grained system as defined above has the same Becker−Döring structure as the original system, namely a Lyapunov function, and conserved quantity: the density. Due to the complex nature of the model

being considered, the contraction will be achieved in a series of stages, rather than in one step as described above.

2.2. Contraction of Model. The reduction of (1.12)−(1.18) to a low-dimensional dynamical system is achieved in a sequence of stages. The first is to replace two-component model for c_r, $f_{r,k}$ by a single-component model for c_r. This model happens to be similar to that of Wattis and Coveney[14] for generalized nucleation in a system with inhibition. The major difference is that the system derived here for vesicle formation has no inhibition; thus there are fewer equations in our reduced model. However, this does not mean that the resulting kinetics are any less complicated. We then coarse-grain this single-component system but do not quite take this process to the ultimate limit of a single variable for the monomer concentration and one for the concentration of vesicles; rather, we retain three concentration variables, one for the monomer concentration and one each for the concentrations of vesicles of two different sizes.

2.3. Reduction to a Single-Component System. We introduce new concentration variables

$$w_r(t) = c_r(t) + \sum_{k=1}^{r} f_{r,k}(t) + \sum_{k=r}^{\infty} f_{k,r}(t) \tag{2.5}$$

which denotes the concentration of all vesicular structures of size r, including complete vesicles whether they have vesicle fragments growing on them or not (that is, c_r and $f_{r,k}$ for $k \le r$), and vesicle fragments of size r (that is $f_{k,r}$ with $k \ge r$). We then have the kinetic equation for w_r

$$\frac{\mathrm{d}w_r}{\mathrm{d}t} = (J_{r-1} + \sum_{k=r}^{\infty} H_{k,r-1}) - (J_r + \sum_{k=r+1}^{\infty} H_{k,r}) \tag{2.6}$$

We thus can write the system as $\dot{w}_r = I_r - I_{r-1}$, which has the familiar Becker−Döring structure where

$$I_r = \epsilon\left(c_r c_1 - \frac{Q_r}{Q_{r+1}} c_{r+1}\right) + \epsilon\gamma \sum_{k=r+1}^{\infty}\left(f_{k,r} c_1 - \frac{Q_r}{Q_{r+1}} f_{k,r+1}\right) \tag{2.7}$$

While retaining the Becker−Döring structure, this system remains vastly complicated and must be approximated further before being contracted. In equilibrium we have that $f_{k,r} \propto c_k c_r$ (1.10) and so we assume that $f_{k,r} \sim \xi c_k c_r$; hence the above expression for I_r can be simplified considerably

$$I_r = \left(c_r c_1 - \frac{Q_r}{Q_{r+1}} c_{r+1}\right)(\epsilon + \epsilon\gamma\xi \sum_{k=r+1}^{\infty} c_k) \tag{2.8}$$

The conversion back to the single variable c_r is also approximate. While the presence of $f_{r,k}$ in the above model is important, particularly to the kinetics because $\epsilon \ll 1$ while $\gamma\epsilon = \mathcal{O}(1)$, each concentration $f_{r,k}$ is also expected to be small ($\xi \ll 1$),[2] so that $c_r \sim w_r$ and we have $\dot{c}_r = I_{r-1} - I_r$ to leading order. We now replace all occurrences of w_r by c_r to obtain the single-component model

$$\dot{c}_r = I_{r-1} - I_r \qquad I_r = \left(c_r c_1 - \frac{Q_r}{Q_{r+1}} c_{r+1}\right)(\epsilon + \epsilon\gamma\xi \sum_{k=r+1}^{\infty} c_k) \tag{2.9}$$

2.4. Coarse-Graining the Single-Component System. As in previous coarse-graining analyses, a size-dependent mesh function $r = \Lambda_n$ may be used instead, and replacing c_r by x_n we gain

$$\dot{x}_n = L_{n-1} - L_n$$

$$\dot{x}_1 = -\lambda_1 L_1 - \sum_{n=1}^{\infty}(\lambda_{n+1}\Lambda_{n+1} - \lambda_n \Lambda_n) L_n \tag{2.10}$$

$$L_n = \left(x_n x_1^{\lambda n} - \frac{Q_{\Lambda_n}}{Q_{\Lambda_{n+1}}} x_{n+1}\right)(\epsilon + \epsilon\gamma\xi \sum_{k=n}^{\infty} x_k)^{\lambda_n} \tag{2.11}$$

For details of the coarse-graining process see Bolton and Wattis[13] and Wattis and Coveney.[14]

2.5. Almost Maximal Reduction. To apply in any particular situation, we need to truncate the system at some maximum size N. If we take very large λ, then this could be as low as $N = 2$ so that we obtain the system

$$\dot{x}_1 = -\lambda(\lambda+1)L, \qquad x_2 = L$$

$$L = (x_1^{\lambda+1} - \beta x_2)(\epsilon + \alpha x_2)^{\lambda} \tag{2.12}$$

where α and β are constants derived from the parameters in the original problem. Even though this system can be reduced to a first-order autonomous ordinary differential equation (by using the conservation of density), it may still display complicated kinetics. Here we study a more complicated approximation to the system; we keep two sizes of cluster, x_2 representing the concentration of smaller sized vesicles (size $\Lambda_2 = \lambda_2 + 1$), and x_3 that of larger vesicles (of size $\Lambda_3 = \lambda_2 + \lambda_3 + 1$). Thus we obtain

$$\dot{x}_1 = -\lambda_2(1+\lambda_2)L_1 - (\lambda_3(1+\lambda_2+\lambda_3) - \lambda_2(1+\lambda_2))L_2 \tag{2.13}$$

$$\dot{x}_2 = L_1 - L_2 \qquad \dot{x}_3 = L_2 \tag{2.14}$$

$$L_1 = (x_1^{\lambda_2+1} - \beta_2 x_2)(\epsilon + \alpha_{12} x_2 + \alpha_{13} x_3)^{\lambda_2} \tag{2.15}$$

$$L_2 = (x_2\, x_1^{\lambda_3} - \beta_3 x_3)(\epsilon + \alpha_{23} x_3)^{\lambda_3} \tag{2.16}$$

where $\alpha_{a,b}$ represents the catalytic influence of a cluster of size Λ_b on the growth of clusters of size Λ_a; these coefficients are derived from the original parameters in the problem. Also β_r is the coarse-grained fragmentation rate derived from the size-dependent form of eq 2.2. We simplify the system of equations (2.13)−(2.16) by eliminating x_1 with the expression for the density, $\rho = x_1 + \lambda_2\Lambda_2 x_2 + \lambda_3\Lambda_3 x_3$; performing this calculation and writing the system explicitly yields the following two-dimensional problem

$$\dot{x}_2 = L_1 - L_2 \qquad \dot{x}_3 = L_2 \tag{2.17}$$

$$L_1 = ((\rho - \lambda_2\Lambda_2 x_2 - \lambda_3\Lambda_3 x_3)^{\lambda_2+1} - \beta_2 x_2)(\epsilon + \alpha_{1,2} x_2 + \alpha_{1,3} x_3)^{\lambda_2} \tag{2.18}$$

$$L_2 = (x_2(\rho - \lambda_2\Lambda_2 x_2 - \lambda_3\Lambda_3 x_3)^{\lambda_3} - \beta_3 x_3)(\epsilon + \alpha_{2,3} x_3)^{\lambda_3} \tag{2.19}$$

which is to be the subject of the rest of this paper. We define the function

$$V = \sum_{r=1}^{3} x_r\left(\log\left(\frac{x_r}{Q_{\Lambda_r}}\right) - 1\right) \tag{2.20}$$

where Q_{Λ_r} is the partition function for the contracted model

defined by

$$Q_{\Lambda_1} = 1 \quad Q_{\Lambda_2} = \frac{1}{\beta_2} \quad Q_{\Lambda_3} = \frac{\beta_2}{\beta_3} \tag{2.21}$$

With V as defined above, it has been shown to qualify as a Lyapunov function for the system and so ensures that the system tends toward a global equilibrium state. With the model contracted we proceed to investigate the system.

3. Asymptotics

With the system reduced to two differential equations, it would be natural to attempt a phase-plane analysis; however, in this case, the highly nonlinear terms hinder this approach. The power of a phase-plane analysis is that it reveals information on all trajectories in phase space. A more limited approach is to solve the system using matched asymptotic expansions, which generates one particular trajectory, and which will yield more detailed results for the chosen initial condition. The essential idea is to consider the system over a series of time scales, in each we retain only those terms that dominate the dynamics over that time scale; rendering the system solvable in each individual time frame. These separate solutions are then "matched" together to ensure a smooth transition from one time frame to the next. For a brief discussion of the theory, see Hinch.[17] We aim to solve the contracted model, given by (2.17)−(2.19), and so must decide specifically how many clusters to group in x_2 and x_3, as given by λ_2 and λ_3, respectively. There are three cases to be considered depending on the relative sizes of λ_2 and λ_3 and in each we impose the initial conditions

$$x_2^{(0)} = \epsilon x_2^{(0)} \qquad x_3^{(0)} = \epsilon x_3^{(0)} \tag{3.1}$$

where $x_2^{(0)}, x_3^{(0)} \sim \mathcal{O}(1)$; hence we assume that the mass of pre-added material is a small quantity, which is in the spirit of the experimental results. We focus on calculating the critical times at which x_2 and x_3 become $\mathcal{O}(1)$ quantities, the dependence of this time on the initial conditions and the relative sizes of x_2 and x_3. The critical times presented in the following analysis are valid for $x_2^{(0)} = x_3^{(0)} = 0$; however, in this case several other time scales are required before attaining the results given here and so for completeness we include a summary of these time scales in Appendix A.

3.1. Case A: $\lambda_3 + 1 < \lambda_2$. The choice of $\lambda_3 + 1 < \lambda_2$ implies that x_2 contains a greater range of cluster sizes than x_3, which represents the larger clusters. An alternative interpretation is that L_1 covers a greater difference in aggregation numbers than L_2.

3.1.1. Time Scale I: $t = \mathcal{O}(\epsilon^{-\lambda_3})$. To focus on the dynamics in the first time scale, we rescale the coordinates; the scalings for x_2 and x_3 are fixed but $t = \epsilon^{\tau} t_1$ and it remains to deduce τ. We determine τ by considering the governing equations to determine which choice will balance the leading order terms and by selecting the fastest time scale. We find either $\tau = \lambda_3$ or $\tau = \lambda_2 - 1$, but $\lambda_3 < \lambda_2 - 1$; so the first option represents the fastest time scale and so

$$x_2 = \epsilon y_2 \quad x_3 = \epsilon(y_3 - y_2) \quad t_1 = \epsilon^{\lambda_3} t \tag{3.2}$$

and the governing equations are

$$\frac{dy_2}{dt_1} = -\epsilon^{\lambda_3+1}(y_2\rho^{\lambda_3} - \beta_3(y_3 - y_2))(1 + \alpha_{2,3}(y_3 - y_2))^{\lambda_3}$$

$$\frac{dy_3}{dt_1} = 0 \tag{3.3}$$

We immediately find $y_3 = x_3^{(0)} + x_2^{(0)}$, but we cannot solve for y_2 explicitly. By inspection of (3.3) we see that

$$y_2 \to \frac{\beta_3(x_3^{(0)} + x_2^{(0)})}{\rho^{\lambda_3} + \beta_3} \qquad \text{as} \qquad t_1 \to \infty \tag{3.4}$$

while y_3 remains constant over the entire time scale. Physically, therefore, we have added an initial amount of x_2 and x_3, which are not necessarily in equilibrium, and so we observe a very fast initial phase where the smaller and larger clusters reach a local equilibrium before any of the mass from the monomers can aggregate up to a significant size, as can be seen by the fact that in this time scale $L_2 = \mathcal{O}(\epsilon^{\lambda_3+1})$, with $L_2 \to 0$ as $t_1 \to \infty$, while $L_1 = \mathcal{O}(\epsilon^{\lambda_2})$ throughout this time scale. At the end of this time scale, x_2 and x_3 remain at the same order of magnitude as at the start, so both will be $\mathcal{O}(\epsilon)$ in the next time scale, and the next time scale will be slower than the current one.

3.1.2. Time Scale II: $t = \mathcal{O}(\epsilon^{1-\lambda_2})$. The next time scale arises from the longer time frame $\tau = \lambda_2 - 1$. We use the scalings

$$x_2 = \epsilon z_2 \quad x_3 = \epsilon(z_3 - z_2) \quad t = \epsilon^{1-\lambda_2} t_2 \tag{3.5}$$

We note that $z_3 - z_2$ must be positive because negative concentrations are not permitted. We find that the dynamics are governed by

$$\epsilon^{\lambda_2}\frac{dz_2}{dt_2} = L_1 - L_2 \sim \mathcal{O}(\epsilon^{\lambda_2}) - \mathcal{O}(\epsilon^{\lambda_3+1})$$

$$\epsilon^{\lambda_2}\frac{dz_3}{dt_2} = L_1 \sim \mathcal{O}(\epsilon^{\lambda_2}) \tag{3.6}$$

Our choice of the form for x_3 now becomes clear, had we taken the obvious choice of $x_3 = \epsilon z_3$, then the RHS of the second equation in (3.6) would have been $L_2 \sim \mathcal{O}(\epsilon^{\lambda_3+1})$, which, to leading order, would have dominated both equations, resulting in the algebraic expression $L_2 = 0$ twice. Using (3.5) the leading order equations are

$$0 = (\rho^{\lambda_3} z_2 - \beta_3(z_3 - z_2))(1 + \alpha_{2,3}(z_3 - z_2))^{\lambda_3} \tag{3.7}$$

$$\frac{dz_3}{dt_2} = \rho^{\lambda_2+1}(1 + \alpha_{1,2}z_2 + \alpha_{1,3}(z_3 - z_2))^{\lambda_2} \tag{3.8}$$

Due to the positive nature of $(z_3 - z_2)$, equation (3.7) results in an algebraic relation, z_2 being slaved to z_3, that is

$$z_2 = \frac{\beta_3 z_3}{\rho^{\lambda_3} + \beta_3} \tag{3.9}$$

and solving the remaining differential equation (3.8) for z_3 yields

$$z_3 = \frac{(\rho^{\lambda_3}+\beta_3)^{\lambda_2/(\lambda_2-1)}}{\rho(\alpha_{1,2}\beta_3+\alpha_{1,3}\rho^{\lambda_3})[(\lambda_2-1)(t_{2c}-t_2)(\alpha_{1,2}\beta_3+\alpha_{1,3}\rho^{\lambda_3})\rho^2]^{1/(\lambda_2-1)}} - \frac{\rho^{\lambda_3}+\beta_3}{\alpha_{1,2}\beta_3+\alpha_{1,3}\rho^{\lambda_3}} \quad (3.10)$$

The constant of integration, t_{2c}, represents the time at which the solutions z_2 and z_3 diverge to infinity. It is curious to note that, counter to intuition, the constant $\alpha_{2,3}$ has no influence on this solution because it was eliminated when solving the algebraic relation (3.7) and does not appear in (3.9). We note that over this time scale $L_2 = 0$ and $L_1 \propto 1/(t_{2c}-t_2)^{\lambda_2/(\lambda_2-1)}$ to leading order; thus, x_2 and x_3 always remain in equilibrium.

Having found the solution in time scale II we must ensure a smooth transition from the previous time scale. We re-express the solution for the first time scale in terms of the variables for the second time scale. Then by considering the limit $t_1 \to \infty$ and the solution from the second time scale in the limit $t_2 \to 0$ we find that the constant t_{2c} is given by

$$t_{2c} = \frac{1}{\rho^{\lambda_2+1}(\lambda_2-1)A[1+A(x_2^{(0)}+x_3^{(0)})]^{\lambda_2-1}} \quad \text{where} \quad A = \frac{\alpha_{1,2}\beta_3+\alpha_{1,3}\rho^{\lambda_3}}{\rho^{\lambda_3}+\beta_3} \quad (3.11)$$

Having completed the analysis for the second time scale, we clearly require a third, because the singularity at $t = t_{2c}$ indicates both x_2 and x_3 reach larger orders of magnitude as $t_2 \to t_{2c}$.

3.1.3. Time Scale III. We must consider the dynamics on a finer time scale about the point $t = t_{2c}$. New elements begin to dominate the governing equations (2.17)−(2.19) when either $x_2 \sim \mathcal{O}(1)$ or $x_3 \sim \mathcal{O}(1)$, which occur at the same time. Taking the limit $t \to t_{2c}$ we obtain from the solutions (3.5), (3.9), and (3.10)

$$x_2 \sim O\left(\frac{1}{(\epsilon^{\lambda_2-1}t_{2c}-t)^{1/\lambda_2-1}}\right) \quad (3.12)$$

new terms from (2.17)−(2.19) become significant when $x_2 \sim \mathcal{O}(1)$; hence we deduce that the new time scale is

$$t = t_3 + t_{2c}\epsilon^{1-\lambda_2} \quad (3.13)$$

which is centered on the singular point of the solution at the end of time scale II and focuses on this region with a much finer time scale than t_2. Note that matching with time scale II occurs as $t_3 \to -\infty$. We have no need to rescale x_2 and x_3 on this time scale as they are of order unity, and so the fluxes written out in full for this time scale are

$$L_1 = ((\rho-\lambda_2\Lambda_2x_2-\lambda_3\Lambda_3x_3)^{\lambda_2+1}-\beta_2x_2)(\alpha_{1,2}x_2+\alpha_{1,3}x_3)^{\lambda_2} \quad (3.14)$$

$$L_2 = (x_2(\rho-\lambda_2\Lambda_2x_2-\lambda_3\Lambda_3x_3)^{\lambda_3}-\beta_3x_3)(\alpha_{2,3}x_3)^{\lambda_3} \quad (3.15)$$

together with (2.17), which unfortunately is not much simpler than the original system (2.17)−(2.19). We cannot solve this explicitly; however, progress is made by considering the phase plane over this time scale and matching the solution from the previous time scale.

The start of the trajectory can be determined by matching with the previous time scale. We re-express the solution from time scale II in terms of x_2, x_3, and t_3; then consider the limit $t_3 \to -\infty$ to obtain the solution in the matching region. This calculation implies that at the start of time scale III the ratio x_2/x_3 is constant, namely

$$\frac{x_2}{x_3} = \frac{\beta_3}{\rho^{\lambda_3}+\beta_3} \quad (3.16)$$

as in (3.9). Crucially, however, neither x_2 or x_3 is zero at the start of time scale III.

Considering the phase plane of the system with fluxes (3.14) and (3.15) we find four steady-state solutions, $\bar{x}_2^{(i)}$, $\bar{x}_3^{(i)}$ $1 \le i \le 4$, namely

$$\text{State I} \quad \begin{cases}(\rho-\lambda_2\Lambda_2\bar{x}_2^{(1)}-\lambda_3\Lambda_3\bar{x}_3^{(1)})^{\lambda_2+1}-\beta_2\bar{x}_2^{(1)}=0\\ (x_2(\rho-\lambda_2\Lambda_2\bar{x}_2^{(1)}-\lambda_3\Lambda_3\bar{x}_3^{(1)})^{\lambda_3}-\beta_3\bar{x}_3^{(1)}=0\end{cases} \quad (3.17)$$

$$\text{State II} \quad \begin{cases}(\rho-\lambda_2\Lambda_2\bar{x}_2^{(2)}-\lambda_3\Lambda_3\bar{x}_3^{(2)})^{\lambda_2+1}-\beta_2\bar{x}_2^{(2)}=0\\ \bar{x}_3^{(2)}=0\end{cases} \quad (3.18)$$

$$\text{State III} \quad \begin{cases}\alpha_{1,2}\bar{x}_2^{(3)}+\alpha_{1,3}\bar{x}_3^{(3)}=0\\ (\bar{x}_2^{(3)}(\rho-\lambda_2\Lambda_2\bar{x}_2^{(3)}-\lambda_3\Lambda_3\bar{x}_3^{(3)})^{\lambda_3}-\beta_3\bar{x}_3^{(3)}=0\end{cases} \quad (3.19)$$

$$\text{State IV} \quad \begin{cases}\bar{x}_2^{(4)}=0\\ \bar{x}_3^{(4)}=0\end{cases} \quad (3.20)$$

State I. We expect the system to be attracted to state I, which is the global equilibrium solution, but it remains for this to be proved and we initially consider this state. We are assured the existence of a Lyapunov function, given by (2.20), whose partial derivatives are

$$\frac{\partial V}{\partial x_2} = \log\left(\frac{\beta_2x_2}{(\rho-\lambda_2\Lambda_2x_2-\lambda_3\Lambda_3x_3)^{\Lambda_2}}\right) \quad (3.21)$$

$$\frac{\partial V}{\partial x_3} = \log\left(\frac{\beta_3x_3}{x_2(\rho-\lambda_2\Lambda_2x_2-\lambda_3\Lambda_3x_3)^{\lambda_3}}\right) \quad (3.22)$$

and so by inspection in state I the Lyapunov function is stationary ($\dot{V}=0$). Furthermore, by investigation of the second derivatives, we conclude that this is a minimum in the Lyapunov function and so this is a stable fixed point.

Finding a locally stable fixed point does not ensure our system will globally tend to this point, we must determine whether any of the other three fixed points have a domain of attraction such that the system may tend to these in this time scale. We further note that $V \to \infty$ as $x_2, x_3 \to \infty$, which ensures that the variables x_2, x_3 do not tend to infinity.

State II. In state II $x_3 = 0$ and x_2 satisfies $\beta_2x_2 = (\rho-\lambda_3\Lambda_3x_3)^{\lambda_2+1}$, which clearly has a unique solution for $x_2 > 0$, located on the boundary of the physically relevant domain $x_2 > 0$, $x_3 > 0$. We linearize the system about the fixed point, using $x_2 = \bar{x}_2^{(2)} + y_2^{(2)}$, $x_3 = \bar{x}_3^{(2)} + y_3^{(2)}$, to yield

$$\begin{pmatrix}\dot{y}_2^{(2)}\\ \dot{y}_3^{(2)}\end{pmatrix} = \begin{pmatrix}T_1 & T_2\\ 0 & 0\end{pmatrix}\begin{pmatrix}y_2^{(2)}\\ y_3^{(2)}\end{pmatrix} + \begin{pmatrix}NL_2\\ NL_3\end{pmatrix} \quad (3.23)$$

where

$$T_1 = (-\Lambda_2{}^2(\rho - \lambda_2\Lambda_2\bar{x}_2^{(2)})^{\lambda_2} - \beta_2)(\alpha_{1,2}\bar{x}_2^{(2)})^{\lambda_2} \quad (3.24)$$

$$T_2 = -\Lambda_2\Lambda_3(\rho - \lambda_2\Lambda_2\bar{x}_2^{(2)})^{\lambda_2}(\alpha_{1,2}\bar{x}_2^{(2)})^{\lambda_2} \quad (3.25)$$

and NL_2, NL_3 are both nonlinear terms. This system has eigenvalues 0 and $T_1 < 0$ with respective eigenvectors $(T_2, -T_1)^T$ and $(1, 0)^T$. Because x_3 is necessarily nonzero when entering the present time scale, then initially we are assured that $y_3^{(2)} > 0$. Calculating the leading order term of $\dot{y}_3^{(2)}$ reveals that

$$\dot{y}_3^{(2)} = \beta_2\bar{x}_2{}^2(\alpha_{2,3}y_3^{(2)})^{\lambda_3} \quad (3.26)$$

and so because β_2, $\alpha_{2,3} \geq 0$ we deduce that the fixed point is unstable to perturbations in the $y_3^{(2)}$ direction. Because $y_3^{(2)}$ is positive at the start of this time scale, we deduce that the system will be outside the domain of attraction for this steady state. We note that this fixed point may influence the dynamics in this time scale.

State III. Eliminating $x_3^{(3)}$ from (3.19), we obtain the solution $x_2 = x_3 = 0$, which will be considered in state IV, or

$$\left(\rho + \left(\lambda_3\Lambda_3\frac{\alpha_{1,2}}{\alpha_{1,3}} - \lambda_2\Lambda_2\right)\bar{x}_2^{(3)}\right)^{\lambda_3} = \frac{-\beta_3\alpha_{1,2}}{\alpha_{1,3}} \quad (3.27)$$

and so if λ_3 is even, then no root exists. Assuming λ_3 to be odd, there are two possibilities: $\alpha_{1,3}\lambda_2\Lambda_2$ is either larger or smaller than $\lambda_2\Lambda_3\alpha_{1,2}$. In the former case then, there exists a root with $\bar{x}_2^{(3)} > 0$, $\bar{x}_3^{(3)} < 0$; otherwise we find $x_2^{(3)} < 0$, $x_3^{(3)} > 0$, where for both cases $\bar{x}_2^{(3)}$, $\bar{x}_3^{(3)} \sim \mathcal{O}(1)$. In both cases the fixed point lies in unphysical space; furthermore, it is outside the physical region by an $\mathcal{O}(1)$ amount and so we ignore this steady state, as the system cannot converge to it.

State IV. Finally, we consider state IV, which is located at the origin. The previous asymptotic analysis is valid for the case $x_2^{(0)}$, $x_3^{(0)} \sim \mathcal{O}(\epsilon)$. So, to consider perturbations about this steady state would in fact be reproducing earlier analysis, where we have demonstrated that a system starting near the origin moves toward positive x_2 and x_3, thus eliminating this as a possible global attractor for the system.

In summary, we have demonstrated that state I is a stable state and, by eliminating the other possibilities, that it is also the global attractor of the system. We note that the time scale for the system to pass through this phase of the dynamics is very short.

3.2. Summary of Time Scale Analysis: $\lambda_3 + 1 < \lambda_2$. Having examined the technical details of matched asymptotics, it is worthwhile to summarize the results that have been obtained. We assumed that $\lambda_3 + 1 < \lambda_2$, so x_2 represents more concentrations than x_3 (that is, the difference in aggregation sizes between x_1 and x_2 is greater than that between x_2 and x_3), and $x_2^{(0)}$, $x_3^{(0)} \sim \mathcal{O}(\epsilon)$. Three relevant time scales have been identified

$$t = \epsilon^{-\lambda_3}t_1 \qquad t = \epsilon^{1-\lambda_2}t_2 \qquad t = t_3 + \epsilon^{1-\lambda_2}t_{2c} \quad (3.28)$$

Initially, x_2 and x_3 reach an equilibrium state before any monomers can aggregate up to a size to affect x_2. Once in this local equilibrium, we enter the second time scale, which spans a long time. Throughout this time scale x_2 and x_3 are in equilibrium because the aggregation of monomers to x_2 is a slow process when compared to the exchange of mass between x_2 and x_3. Most of the mass exists as monomers; however, a sufficient amount has aggregated to higher cluster sizes to catalyze the aggregation of monomers into both small and large vesicles. As this process gathers pace, we find that both x_2 and x_3 become $\mathcal{O}(1)$ at a critical time, t_{2c}, signaling the end of this time scale, and in time scale III an appreciable number of monomers have been depleted; further aggregation is dominated by the catalytic effect. It only remains for the system to tend to its final equilibrium state. It is curious to note that the catalytic effect of x_3 on the clusters in x_2, as given by $\alpha_{2,3}$, has no influence on the solution in the regime $\lambda_3 + 1 < \lambda_2$, which may be attributed to the fact that x_2 and x_3 equilibrate before the catalytic effect between them exerts any influence on the dynamics. The main result of this analysis is that t_{2c}, the critical time when x_2, $x_3 \sim \mathcal{O}(1)$ is dependent on the initial conditions $x_2^{(0)}$, $x_3^{(0)}$ and that by increasing the amount of mass in x_2, x_3, initially the time taken for these coordinates to reach $\mathcal{O}(1)$ is decreased significantly (see (3.11) for the detailed formula for t_{2c}).

3.3. Case B: $\lambda_2 < \lambda_3 + 1$. Having previously investigated the case where the range of sizes of vesicles in x_2 exceeds those in x_3, we now consider the reverse situation ($\lambda_2 < \lambda_3 + 1$). Now x_2 represents clusters of a much smaller range of aggregation numbers ($2 \leq r \leq \lambda_2 + 1$), much closer to the size of a monomer, than those clusters in x_3 ($\lambda_2 + 2 \leq r \leq \lambda_2 + \lambda_3 + 1$). More formally, we examine the region where $\lambda_2 < \lambda_3 + 1$. We use the same initial conditions as for the previous case (3.1) and proceed to investigate the resulting time scales.

3.3.1. Time Scale I. The scalings for x_2 and x_3 are defined by the initial conditions; however, choice still remains about the time scale, and so we define $t = \epsilon^{-\tau}t_1$ and select the fastest time scale to be considered first; thus we deduce that $\tau = \lambda_2 - 1$ and hence

$$x_2 = \epsilon y_2 \qquad x_3 = \epsilon y_3 \qquad t = \epsilon^{-\lambda_2+1}t_1 \quad (3.29)$$

In this time scale

$$\frac{dy_2}{dt_1} = \rho^{\lambda_2+1}(1 + \alpha_{1,2}y_2 + \alpha_{1,3}y_3)^{\lambda_2} \qquad \frac{dy_3}{dt_1} = 0 \quad (3.30)$$

which immediately yields the solution

$$y_2 = \frac{1}{[\alpha_{1,2}(\lambda_2 - 1)\alpha_{1,2}\rho^{\lambda_2+1}(t_{1c} - t_1)]^{1/(\lambda_2-1)}} - \frac{1+\alpha_{1,3}\,x_3^{(0)}}{\alpha_{1,2}} \quad (3.31)$$

$y_3 = x_3^{(0)}$ where t_{1c} is a constant of integration; by imposing the initial condition, we find

$$t_{1c} = \frac{1}{((\lambda_2 - 1)\alpha_{1,2}\rho^{\lambda_2+1}[1 + \alpha_{1,2}x_2^{(0)} + \alpha_{1,3}\,x_3^{(0)}]^{\lambda_2-1})^{1/(\lambda_2-1)}} \quad (3.32)$$

Note that t_{1c} depends sensitively on the initial conditions, and as $t \to t_{1c}$, y_2 tends to infinity and a new time scale is required. In terms of the fluxes we have $L_2 = \mathcal{O}(\epsilon^{\lambda_3+1})$ throughout this time scale and $L_1(0) = \mathcal{O}(\epsilon^{\lambda_2})$, but with $L_1 \propto 1/(t_{1c} - t_1)^{\lambda_2/(\lambda_2-1)}$ as $t_1 \to t_{1c}$; thus in the second time scale x_2 will be larger than $\mathcal{O}(\epsilon)$ whereas x_3 will remain $\mathcal{O}(\epsilon)$.

3.3.2. Time Scale II. The previous time scale ends when $x_2 \sim \mathcal{O}(1)$, and from (3.31) we deduce that this occurs when $t - \epsilon^{1-\lambda_2}t_{1c} \sim \mathcal{O}(1)$; so we rescale the coordinates by

$$x_2 = z_2 \quad x_3 = \epsilon z_3 \quad t = \epsilon^{1-\lambda_2}t_{1c} + t_2 \quad (3.33)$$

and the governing equations for this time scale are

$$\frac{dz_2}{dt_2} = ((\rho - \lambda_2\Lambda_2 z_2)^{\lambda_2+1} - \beta_2 z_2)(\alpha_{1,2} z_2)^{\lambda_2} \quad \frac{dz_3}{dt_2} = 0 \quad (3.34)$$

It is clear that z_3 does not change over this time scale, and so, by matching, we obtain $z_3 = x_3^{(0)}$. The dynamics for z_2 (3.34) are not explicitly tractable, however, because $\alpha_{1,2}z_2 > 0$ at the end of this time scale; namely, as $t_2 \to \infty$, we have $z_2 \to x_{2\mathrm{con}}$, where $x_{2\mathrm{con}}$ satisfies

$$(\rho - \lambda_2\Lambda_2 x_{2\mathrm{con}})^{\Lambda_2} - \beta_2 x_{2\mathrm{con}} = 0 \quad (3.35)$$

that is, the x_2 clusters equilibrate with the monomers over this time scale and we note that this occurs before any significant amount of mass aggregates to x_3. It is clear that again $L_2 = \mathcal{O}(\epsilon^{\lambda_3})$ over this time scale but also at the start of the time scale $L_1 = \mathcal{O}(\epsilon^{\lambda_2})$ with $L_1 \to 0$ as $t_2 \to \infty$.

3.3.3. Time Scale III. Over the previous time scale the dynamics appear to have stopped; however, if we now consider a slower time scale, we find that the system is changing, but by mechanisms that occurred too slowly to be observable on the last time scale, namely, the flux L_2. We now choose a time scale such that the dx_3/dt term is balanced by this and we scale according to

$$x_2 = p_2 \quad x_3 = \epsilon p_3 \quad t = t_3\epsilon^{2-\lambda_2} + t_{1\mathrm{c}}\epsilon^{1-\lambda_2} \quad (3.36)$$

hence we must solve

$$0 = ((\rho - \lambda_2\Lambda_2 p_2)^{\lambda_2+1} - \beta_2 p_2)(\alpha_{1,2} p_2)^{\lambda_2} \quad (3.37)$$

$$\frac{dp_3}{dt_3} = p_2(\rho - \lambda_2\Lambda_2 p_2)^{\lambda_3}(1 + \alpha_{1,3}p_3)^{\lambda_3} \quad (3.38)$$

We immediately deduce that $p_2 = x_{2\mathrm{con}}$ for the entire time scale, substituting this into (3.38) and solving reveals

$$p_3 = \frac{1}{\alpha_{2,3}}\left[\frac{1}{[\alpha_{2,3}(\lambda_3 - 1)x_{2\mathrm{con}}(\rho - \lambda_2\Lambda_2 x_{2\mathrm{con}})^{\lambda_3}(t_{3\mathrm{c}} - t_3)]^{1/(\lambda_3-1)}} - 1\right] \quad (3.39)$$

where we determine the constant $t_{3\mathrm{c}}$ by matching into time scale II. The solution for x_3 in time scale II is the constant, $x_3^{(0)}$, considering (3.39) in the limit $t_3/t_{3\mathrm{c}} \to 0$ yields

$$t_{3\mathrm{c}} = \frac{1}{(\lambda_3 - 1)\alpha_{2,3}x_{2\mathrm{con}}(\rho - \lambda_2\Lambda_2 x_{2\mathrm{con}})^{\lambda_3}(1 + \alpha_{2,3}x_3^{(0)})^{\lambda_3-1}} \quad (3.40)$$

Having determined the time at which $p_3 \to \infty$ we instigate a finer time scale about this point to describe the dynamics. Over this time scale $L_1 = 0$ as x_1 and x_2 have reached a local equilibrium state, while $L_2 = \mathcal{O}(\epsilon^{\lambda_3})$ with $L_2 \propto (t_{3\mathrm{c}} - t_3)^{-\lambda_3/(\lambda_3-1)}$ as $t_3 \to t_{3\mathrm{c}}$.

3.3.4. Time Scale IV. As $t_3 \to t_{3\mathrm{c}}$ the solution diverges, indicating that x_3 becomes $\mathcal{O}(1)$ and so we require another time scale with the scalings

$$x_2 = q_2 \quad x_3 = q_3 \quad t = t_4 + \epsilon^{1-\lambda_3}t_{3\mathrm{c}} + \epsilon^{1-\lambda_2}t_{1\mathrm{c}} \quad (3.41)$$

We note that the governing equations will be the same as for the analysis in section 3.1.3; hence we state that the system converges to its equilibrium configuration (state I) over this fast time scale.

3.4. Summary of Time Scale Analysis: $\lambda_2 < \lambda_3 + 1$. The addition of an $\mathcal{O}(\epsilon)$ amount of pre-added material to x_2 and x_3 initially is intended to simulate the templating experiments. In this case comparisons between the templating and nontemplating cases will not be as clear as when $\lambda_3 + 1 < \lambda_2$ because we now have two critical times, one for x_2 and x_3, respectively. The critical times are when either variable grows to $\mathcal{O}(1)$ and represents the time at which the concentration would be sufficiently large to detect experimentally. We observe that x_2 reaches $\mathcal{O}(1)$ before x_3 due to the mass from the monomers aggregating to x_2 faster than to x_3. We developed the solution through four time scales

$$t = \epsilon^{1-\lambda_2}t_1 \qquad t = \epsilon^{1-\lambda_2}t_{1\mathrm{c}} + t_2 \qquad t = \epsilon^{1-\lambda_2}t_{1\mathrm{c}} + \epsilon^{1-\lambda_3}t_3 \quad (3.42)$$

The first is a slow time scale over which the x_2 concentration rises and the x_3 concentration remains constant. As t_1 approaches the first critical time, $t_{1\mathrm{c}}$, x_2 becomes $\mathcal{O}(1)$, where $t_{1\mathrm{c}}$ is given by (3.32). This critical time is greatly reduced by the addition of either x_2 or x_3 initially. Over the fast, second, time scale x_3 remains constant and x_2 tends to a local equilibrium state with the monomer concentration. During the third time scale, which is slower than the first, x_2 remains in local equilibrium with the monomer concentration but the production of x_3 gathers pace and eventually $x_3 \sim \mathcal{O}(1)$ when $t \to \epsilon^{1-\lambda_3}t_{3\mathrm{c}} + \epsilon^{1-\lambda_2}t_{1\mathrm{c}}$, with $t_{3\mathrm{c}}$ given by (3.40). If $x_2^{(0)} \neq 0$, then this will have a strong influence on the time $t_{1\mathrm{c}}$ over which x_2 becomes observable, but there will be no influence on the time $t_{3\mathrm{c}}$. One final, fast, phase is observed over which the system tends toward the global equilibrium.

3.5. Case C: $\lambda_2 = \lambda_3 + 1$. The above analysis is valid for a wide range of λ_2 and λ_3, with the notable exception of $\lambda_3 + 1 = \lambda_2$. Physically, this case represents the situation where the difference in sizes represented by x_2 and x_3 is the same as between x_1 and x_2. The dynamics of the system is finely balanced such that the form of the solution is remarkably different from both $\lambda_2 < \lambda_3 + 1$ and $\lambda_3 + 1 < \lambda_2$; between these regions we expect a structure of time scales that "crossover" from one regime to the other.

In the case of $\lambda_3 + 1 = \lambda_2$ we find that the appropriate scalings for the first time scale are

$$x_2 = \epsilon y_2 \quad x_3 = \epsilon y_3 \quad t = \epsilon^{-\lambda_3}t_1 = \epsilon^{1-\lambda_2}t_1 \quad (3.43)$$

and we obtain the governing equations

$$\frac{dy_2}{dt_1} = \rho^{\lambda_3+2}(1 + \alpha_{1,2}y_2 + \alpha_{1,3}y_3)^{\lambda_3+1} - \rho^{\lambda_3}y_2(1 + \alpha_{2,3}y_3)^{\lambda_3} + \beta_3 y_3(1 + \alpha_{2,3}y_3)^{\lambda_3} \quad (3.44)$$

$$\frac{dy_3}{dt_1} = \rho^{\lambda_3}y_2(1 + \alpha_{2,3}y_3)^{\lambda_3} - \beta_3 y_3(1 + \alpha_{2,3}y_3)^{\lambda_3} \quad (3.45)$$

which cannot be solved analytically due to the strong nonlinear terms that have not been eliminated by the scalings. We illuminate the breakdown of the asymptotic approach in this special case by considering the scalings in the regions adjacent to $\lambda_3 + 1 = \lambda_2$.

If $\lambda_2 > \lambda_3 + 1$, then x_2 and x_3 both grow to $\mathcal{O}(1)$ over the same time scale, maintaining a local equilibrium. If $\lambda_2 < \lambda_3 + 1$, then $x_2 \to \mathcal{O}(1)$, followed by $x_3 \to \mathcal{O}(1)$ in a later time scale; subsequently these equilibrate. In the special case $\lambda_2 = \lambda_3 + 1$ the two possible time scales, $t = \epsilon^{-\lambda_3} t_1$ and $t = \epsilon^{1-\lambda_2}$, merge and we have both x_2 and x_3 growing to $\mathcal{O}(1)$ and equilibrating on the same time scale, but the system remains intractable. However, by demonstrating that the two limiting cases tend to the same scheme, we support the view that this is the only matching region between them.

4. Phase Plane Analysis

As mentioned at the start of section 3, phase-plane analysis brings another dimension to our understanding of the system because it reveals the dynamics for arbitrary initial conditions. However, the strongly nonlinear nature of the problem hinders this approach, as we shall see below, but the asymptotic results given above help us interpret the phase plane.

In a similar way to section 3.1.3 we wish to investigate the critical points of the system, but here we will consider the original system, (2.17)−(2.19), rather than the leading-order approximation valid in the final time scale. For a critical point we require that both L_1 (2.18) and L_2 (2.19) be zero, which implies the existence of four distinct critical points $\bar{x}_2^{(i)}, \bar{x}_3^{(i)}$ $1 \le i \le 4$, namely

State I

$$\begin{cases} [\rho - \lambda_2(\lambda_2+1)\bar{x}_2^{(1)} - \lambda_3(\lambda_2+\lambda_3+1)\bar{x}_3^{(1)}]^{\lambda_2+1} - \beta_2 \bar{x}_2^{(1)} = 0 \\ \bar{x}_2^{(1)}[\rho - \lambda_2(\lambda_2+1)\bar{x}_2^{(1)} - \lambda_3(\lambda_2+\lambda_3+1)\bar{x}_3^{(1)}]^{\lambda_3} - \beta_3 \bar{x}_3^{(1)} = 0 \end{cases} \tag{4.1}$$

State II

$$\begin{cases} [\rho - \lambda_2(\lambda_2+1)\bar{x}_2^{(2)} - \lambda_3(\lambda_2+\lambda_3+1)\bar{x}_3^{(2)}]^{\lambda_2+1} - \beta_2 \bar{x}_2^{(2)} = 0 \\ \epsilon + \alpha_{2,3}\bar{x}_3^{(2)} = 0 \end{cases} \tag{4.2}$$

State III

$$\begin{cases} \epsilon + \alpha_{1,2}\bar{x}_2^{(3)} + \alpha_{1,3}\bar{x}_3^{(3)} = 0 \\ \bar{x}_2^{(3)}[\rho - \lambda_2(\lambda_2+1)\bar{x}_2^{(3)} - \lambda_3(\lambda_2+\lambda_3+1)\bar{x}_3^{(3)}]^{\lambda_3} - \beta_3 \bar{x}_3^{(3)} = 0 \end{cases} \tag{4.3}$$

State IV

$$\begin{cases} \epsilon + \alpha_{1,2}\bar{x}_2^{(4)} + \alpha_{1,3}\bar{x}_3^{(4)} = 0 \\ \epsilon + \alpha_{2,3}\bar{x}_3^{(4)} = 0 \end{cases} \tag{4.4}$$

and we will analyze these in turn and then apply the knowledge gained from the matched asymptotic analysis to the result.

4.1. State I. For this fixed point we have the conditions (4.1) and so the location of this fixed point is undetermined; however, we have that $\bar{x}_2^{(1)} \sim \mathcal{O}(1)$ to balance the ρ^{λ_2+1} term in the first condition, which in turn implies that $\bar{x}_3^{(1)} \sim \mathcal{O}(1)$ from the second. Linerising about the fixed point yields

$$\begin{pmatrix} \dot{y}_2^{(1)} \\ \dot{y}_3^{(1)} \end{pmatrix} = \begin{pmatrix} R_1 - S_1 & R_2 - S_2 \\ S_1 & S_2 \end{pmatrix} \begin{pmatrix} y_2^{(1)} \\ y_3^{(1)} \end{pmatrix} + \begin{pmatrix} NL_2^1 \\ NL_3^1 \end{pmatrix} \tag{4.5}$$

where

$$R_1 = -({\Lambda_2}^2 (x_1^{(1)})^{\Lambda_2 - 1} - \beta_2)(\epsilon + \alpha_{1,2}\bar{x}_2^{(1)} + \alpha_{1,3}\bar{x}_3^{(1)})^{\lambda_2} \tag{4.6}$$

$$R_2 = -(\Lambda_3 \Lambda_2 (x_1^{(1)})^{\Lambda_2 - 1} - \beta_2)(\epsilon + \alpha_{1,2}\bar{x}_2^{(1)} + \alpha_{1,3}\bar{x}_3^{(1)})^{\lambda_2} \tag{4.7}$$

$$S_1 = (x_1^{(1)})^{\lambda_3}\left(1 - \frac{\Lambda_2 \lambda_3 x_2^{(1)}}{x_1^{(1)}}\right)(\epsilon + \alpha_{2,3}\bar{x}_3^{(1)})^{\lambda_3} \tag{4.8}$$

$$S_2 = -(\beta_3 + \Lambda_3 \lambda_3 x_2^{(1)} x_1^{(1)})(\epsilon + \alpha_{2,3}\bar{x}_3^{(1)})^{\lambda_3} \tag{4.9}$$

where the coordinate $x_1^{(1)}$ has been reintroduced to simplify the algebra. By the Routh−Hurwitz condition, (for example see ref 19), both eigenvalues of the linear system have negative real parts because the relations $S_1 - S_2 - R_2 > 0$ and $S_2 R_1 - R_2 S_1 > 0$ can easily be verified. Thus we are assured that this critical point is a stable fixed point.

4.2. State II. From the conditions (4.2) we deduce that $\bar{x}_3^{(2)}$ is small, $\mathcal{O}(\epsilon)$, and negative. We determine $\bar{x}_2^{(2)}$ from the condition

$$(\rho - \Lambda_2 \bar{x}_2^{(2)})^{\Lambda_2} - \beta_2 \bar{x}_2^{(2)} \approx 0 \tag{4.10}$$

thus $\bar{x}_2^{(2)}$ is $\mathcal{O}(1)$ and positive, we linearize about the fixed point to yield

$$\begin{pmatrix} \dot{y}_2^{(2)} \\ \dot{y}_3^{(2)} \end{pmatrix} = \begin{pmatrix} Q_1 & Q_2 \\ 0 & 0 \end{pmatrix} \begin{pmatrix} y_2^{(2)} \\ y_3^{(2)} \end{pmatrix} + \begin{pmatrix} (E y_3^{(2)})^{\lambda_3} \\ -(E y_3^{(2)})^{\lambda_3} \end{pmatrix} \tag{4.11}$$

where

$$Q_1 = -{\Lambda_2}^2(\rho - \lambda_2 \Lambda_2 \bar{x}_2^{(2)} - \lambda_3 \Lambda_3 \bar{x}_3^{(2)})^{\Lambda_2 - 1} - \beta_2(\epsilon + \alpha_{1,2}\bar{x}_2^{(2)} + \alpha_{1,3}\bar{x}_3^{(2)})^{\lambda_2} \tag{4.12}$$

$$Q_2 = -\Lambda_2 \Lambda_3(\rho - \lambda_2 \Lambda_2 \bar{x}_2^{(2)} - \lambda_3 \Lambda_3 \bar{x}_3^{(2)})^{\Lambda_2 - 1}(\epsilon + \alpha_{1,2}\bar{x}_2^{(2)} + \alpha_{1,3}\bar{x}_3^{(2)})^{\lambda_2} \tag{4.13}$$

$$E = -[\bar{x}_2^{(2)}(\rho - \lambda_2 \Lambda_2 \bar{x}_2^{(2)} - \lambda_3 \Lambda_3 \bar{x}_3^{(2)})^{\lambda_3} - \beta_3 \bar{x}_3^{(2)}]\alpha_{2,3}^{\lambda_3} \tag{4.14}$$

We note that $E < 0$. From the conditions defining the fixed point Q_1, Q_2 in (4.12) and (4.13) we deduce that both Q_1 and Q_2 must be negative. The linear matrix has eigenvalues 0 and Q_1 with eigenvectors $(Q_2, -Q_1)^{\mathrm{T}}$ and $(1, 0)^{\mathrm{T}}$, respectively, and so once again there exists a stable center manifold to which the system is attracted ($Q_1 < 0$). We transform the coordinates, to diagonalize the linear matrix, using $u = Q_1 y_2^{(2)} + Q_2 y_3^{(2)}$, $v = y_3^{(2)}$, and hence obtain

$$\begin{pmatrix} \dot{u} \\ \dot{v} \end{pmatrix} = \begin{pmatrix} Q_1 & 0 \\ 0 & 0 \end{pmatrix} \begin{pmatrix} u \\ v \end{pmatrix} + \begin{pmatrix} (Q_1 - Q_2) E v^{\lambda_3} \\ -E v^{\lambda_3} \end{pmatrix} \tag{4.15}$$

The center manifold is given by $u = (Q_1 - Q_2) E v^{\lambda_3}/Q_1$. Transforming back to the coordinates y_2 and y_3 reveals that the center manifold is given by

$$y_2^{(2)} \approx -\frac{Q_2}{Q_1} y_3^{(2)} + \left(\frac{1 - \frac{Q_2}{Q_1}}{Q_1}\right)(-E)(y_3^{(2)})^{\lambda_3} \tag{4.16}$$

Hence the leading order term in the center manifold implies a line with negative slope. In addition, E is also negative but the sign of the correction term is still undetermined and depends on the relative sizes of Q_1 and Q_2. If $Q_2 < Q_1$, then the correction term is negative, and so as y_3 increases, there will be a downward curve on the leading order solution; if $Q_1 < Q_2$ the reverse is true. From the definitions of these quantities it is not possible to state which situation prevails in general. We know

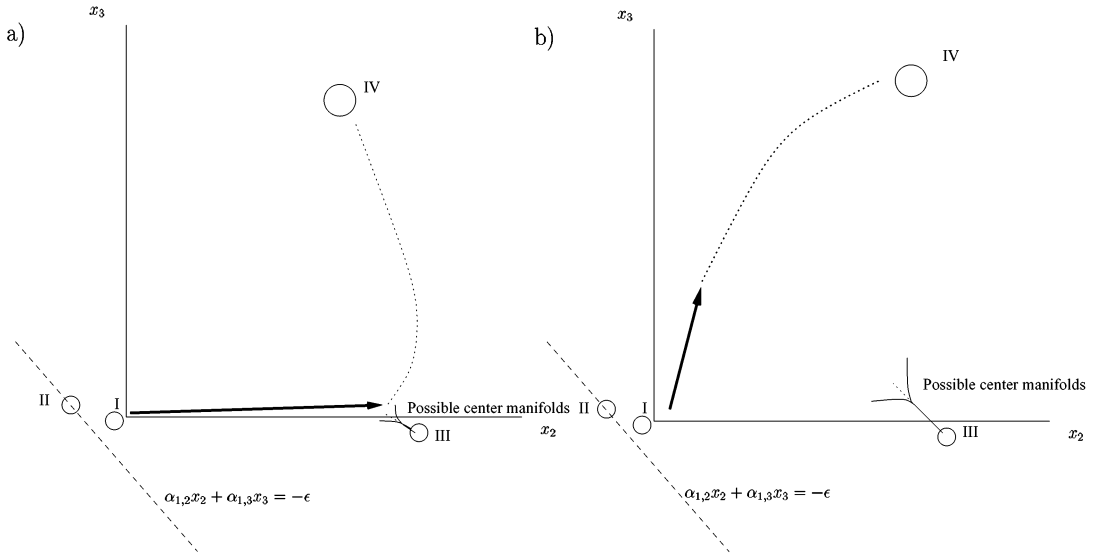

Figure 3. (a) Summary of the effect of the fixed points in the phase plane for the case $\lambda_2 < \lambda_3 + 1$. (b) Summary of the effect of the fixed points in the phase plane for the case $\lambda_3 + 1 < \lambda_2$.

that $\dot{v} = -Ev^{\lambda_3}$, and because $E < 0$, we are assured that the motion along the center manifold will be away form the fixed point.

4.3. State III. We solve (4.3) asymptotically in the limit $\epsilon \rightarrow 0$ to find

$$\bar{x}_2^{(3)} \sim \frac{-\epsilon\beta_3}{\alpha_{1,2}\beta_3 + \alpha_{1,3}\rho^{\lambda_3}} \qquad \bar{x}_3^{(3)} \sim \frac{-\epsilon\rho^{\lambda_3}}{\alpha_{1,2}\beta_3 + \alpha_{1,3}\rho^{\lambda_3}} \quad (4.17)$$

We note that if λ_3 is odd and $\Lambda_3\alpha_{1,2} < \Lambda_2\alpha_{1,3}$ other solutions exist, where typically $\bar{x}_2^{(3)}$ and $\bar{x}_3^{(3)}$ are $\mathcal{O}(1)$ quantities and we are assured that either $\bar{x}_2^{(3)} < 0$ or $\bar{x}_3^{(3)} < 0$ and so these solutions lie away from the physically relevant region (x_2, $x_3 > 0$) and so these are ignored. Linearizing about the fixed point yields $\dot{y}_2^{(3)}$

$$\begin{pmatrix}\dot{y}_2^{(3)}\\ \dot{y}_3^{(3)}\end{pmatrix} = \begin{pmatrix}-T_1 & -T_2\\ T_1 & T_2\end{pmatrix}\begin{pmatrix}y_2^{(3)}\\ y_3^{(3)}\end{pmatrix} + \begin{pmatrix}NL_2^3\\ NL_3^3\end{pmatrix} \quad (4.18)$$

where

$$T_1 = [(\rho - \lambda_2\Lambda_2\bar{x}_2^{(3)} - \lambda_3\Lambda_3\bar{x}_3^{(3)})^{\lambda_3} - \lambda_3\Lambda_2\bar{x}_2^{(3)}(\rho - \lambda_2\Lambda_2\bar{x}_2^{(3)} - \lambda_3\Lambda_3\bar{x}_3^{(3)})^{\lambda_3-1}](\epsilon + \alpha_{2,3}\bar{x}_3^{(3)})^{\lambda_3}$$

$$T_2 = (-\Lambda_3\lambda_3\bar{x}_2^{(3)}(\rho - \lambda_2\Lambda_2\bar{x}_2^{(3)} - \lambda_3\Lambda_3\bar{x}_3^{(3)})^{\lambda_3-1} - \beta_3)(\epsilon + \alpha_{2,3}\bar{x}_3^{(3)})^{\lambda_3} \quad (4.19)$$

if $\bar{x}_2^{(3)}$, $\bar{x}_3^{(3)} \sim \mathcal{O}(\epsilon)$ then $T_1 > 0$ and $T_2 < 0$. The linear part of the system has eigenvalues 0 and $T_2 - T_1$ corresponding to eigenvectors $(T_2, -T_1)^T$ and $(-1, 1)^T$, respectively. The existence of an eigenvector with zero eigenvalue in turn implies the existence of a center manifold[18] that is stable because $T_2 - T_1 < 0$. As with state IV, state III is very close to the origin, so once x_2 and x_3 reach $\mathcal{O}(1)$ in size, the effect of this critical point will be minimal.

4.4. State IV. The position of the final critical point, $(\bar{x}_2^{(4)}, \bar{x}_3^{(4)})$, is given by

$$\bar{x}_2^{(4)} = \frac{\epsilon}{\alpha_{1,2}}\left(-1 + \frac{\alpha_{1,3}}{\alpha_{2,3}}\right) \qquad \bar{x}_3^{(4)} = -\frac{\epsilon}{\alpha_{2,3}} \quad (4.20)$$

and so $\bar{x}_2^{(4)}$ and $\bar{x}_3^{(4)}$ are both $\mathcal{O}(\epsilon)$. We note that because $\bar{x}_3^{(4)} < 0$ this critical point lies outside the physically possible region. We linearize around the critical point and we find that there is no linear part to the dynamics; however, we rely on the fact that the asymptotic analysis provides a solution in which $\dot{x}_2 > 0$ and $\dot{x}_3 > 0$, so this state is unstable; and the dominance of nonlinear terms explains the slow dynamics for initial conditions near $x_2 = x_3 = 0$.

4.5. Case $\lambda_2 < \lambda_3 + 1$. In this case we know that as x_2 becomes $\mathcal{O}(1)$ x_3 remains very small. When x_2 has equilibrated with the monomer concentration, until to leading order it has the same value as $\bar{x}_2^3$, the x_3 concentration grows to $\mathcal{O}(1)$. We postulate that it is the third critical point, from which a center manifold emerges, whose influence not only forces the system toward the equilibrium point but also alters the time scales involved. Motion near a fixed point is much slower than far from it and so we attribute the separation of the time for x_2 and x_3 to grow to $\mathcal{O}(1)$ to the fact that the system approaches close to the third fixed point, when $x_2 \sim \mathcal{O}(1)$ and $x_3 \sim \mathcal{O}(\epsilon)$, which slows the dynamics in this region. We sketch the situation in Figure 3a. The path from I to III takes place on an $\mathcal{O}(\epsilon^{1-\lambda_2})$ time scale and for III to IV an $\mathcal{O}(\epsilon^{1-\lambda_3})$ time scale.

4.6. Case $\lambda_3 + 1 < \lambda_2$. We have learned from the analysis in section 3 that, in the case where $\lambda_3 + 1 < \lambda_2$, x_2 and x_3 both become $\mathcal{O}(1)$ over the same time scale, and both are fixed in a particular ratio, namely $\beta_3 x_3 = (\beta_3 + \rho^{\lambda_3})x_2$. We know the position of the equilibrium state from (4.1) and deduce that

$$\frac{\bar{x}_3^{(4)}}{\bar{x}_2^{(4)}} = \frac{(\rho - \lambda_2\Lambda_2\bar{x}_2^{(4)} - \lambda_3\Lambda_3\bar{x}_3^{(4)})^{\lambda_3}}{\beta_3} \quad (4.21)$$

and so the equilibrium point lies below the line traced by the solution as x_2 and x_3 become $\mathcal{O}(1)$; this is sketched in Figure 3b.

This situation is almost identical for a variety of initial conditions, if the initial amount of mass in x_2 and x_3 is $\mathcal{O}(\epsilon)$, but the time taken to travel this path is decreased if more mass is pre-added. So in this case only the fourth fixed point has had any impact on the dynamics.

5. Conclusion

Having reviewed the experimental literature on vesicle growth, particularly in the presence of pre-added vesicles, we note that a catalytic process occurs which gives rise to a variety of phenomena, including the size templating matrix effect. Previously we proposed a microscopic model to describe this, based on the Becker−Döring equations.[3] The size of the system, and the strong nonlinearity, precludes a direct analytical approach to such a detailed model and we relied on numerical simulations. In this paper we present a low-dimensional approximation to the microscopic model, based on an established coarse-graining procedure. When applying such a method we have a choice on how to reduce the many concentrations into three variables: we chose x_1 to represent the monomers, x_2 the smallest λ_2 clusters, and x_3 the remaining λ_3 clusters. We have solved this system using matched asymptotics. The structure of the solution depends on the relative size of λ_2 and λ_3; three different types of behavior are observed, depending on the relative sizes of λ_2 and λ_3, namely, $\lambda_3 + 1 < \lambda_2$, $\lambda_2 < \lambda_3 + 1$, and $\lambda_2 = \lambda_3 + 1$. The special case $\lambda_2 = \lambda_3 + 1$ being a matching case between the two generic structures.

Because pre-adding vesicles in both x_2 and x_3, or x_2 and x_3, is not particularly instructive, we discuss four systems. First we consider the region $\lambda_3 + 1 < \lambda_2$; that is, x_2 represents a broader range of cluster sizes than x_3. Case I: From initial conditions $x_1 \sim \mathcal{O}(1)$, $x_2 \sim \mathcal{O}(\epsilon)$, and $x_3 = 0$ we find that x_2 and x_3 equilibrate over a fast time scale and then on a slower time scale the monomers aggregate to larger cluster sizes. Alternatively, case II has initial conditions $x_1 \sim \mathcal{O}(1)$, $x_2 = 0$, and $x_3 \sim \mathcal{O}(\epsilon)$; again, x_2 and x_3 equilibrate rapidly, followed by a slower time scale over which the monomeric mass aggregates to the larger cluster sizes. In both cases x_2 and x_3 grow to $\mathcal{O}(1)$ over the same time scale and the dynamics are dominated by the fact that the clusters represented by x_2 are, on average, closer in aggregation number to x_3 than the monomers.

In the region $\lambda_2 < \lambda_3 + 1$ we have x_2 representing a smaller range of cluster sizes than x_3; that is, x_2 represents, on average, clusters of a size more similar to a monomer than those in x_3. Case III has initial conditions $x_1 \sim \mathcal{O}(1)$, $x_2 \sim \mathcal{O}(\epsilon)$, and $x_3 = 0$. At relatively short times x_1 and x_2 equilibrate and $x_2 \sim \mathcal{O}(1)$ whereas x_3 remains zero to leading order; this process is accelerated by the initial presence of x_2 clusters. Over a longer time scale mass aggregates to larger cluster sizes, while maintaining a local equilibrium between x_1 and x_2: the time scale for this process is the same regardless of the mass pre-added in x_2. In case IV we have initial conditions $x_1 \sim \mathcal{O}(1)$, $x_2 = 0$, and $x_3 \sim \mathcal{O}(\epsilon)$. Again, we observe x_1 and x_2 rapidly equilibrating, in this case accelerated by the x_3 clusters, which also causes the longer time scale, for x_3 to grow to $\mathcal{O}(1)$, to be reduced.

Case III illustrates the size-templating effect best; in this case only small vesicles are pre-added. After a fast phase we find that the concentration of x_2 has reached $\mathcal{O}(1)$ whereas x_3 remains essentially zero. Hence, mass has aggregated to the same size, or smaller, than the pre-added vesicles over this short time scale, which is the experimentally observed result. Over a much slower time scale the system reaches the global equilibrium solution and the length of this time scale is unaffected by the presence of pre-added vesicles. In all cases we expect the pre-added vesicles to form the larger clusters in the final distribution, in agreement with the experimental evidence presented in Figure 1.

To develop a more general understanding of the model, we analyzed the (x_2, x_3) phase plane. Identifying four fixed points we eliminated three by deducing that they were outside the physical domain and that the asymptotics established that for a range of initial conditions the system moved away from these points, two are very close to the origin. The fourth fixed point was identified as the global attractor for the system. From the third fixed point a center manifold emerges into the physical domain onto which the local dynamics is forced by the linear part of the governing equations: when $\lambda_2 < \lambda_3 + 1$, despite being outside the physical domain, this center manifold plays a role in the dynamics of the system. Not only does this fixed point alter the path of the system, but as this path passes close to the fixed point it also slows the dynamics, thus separating the times for x_2 and x_3 to reach $\mathcal{O}(1)$. This analysis demonstrates the importance of nonlinear dynamics in the kinetics of the size-templating effect.

The experiments and model presented here are important to the problem of the chemical origins of life. As bounded cell-like structures that form spontaneously, given adequate conditions, vesicles have recently attracted considerable investigation; demonstrating an ability for size-templating serves to increase this interest. We find the size-templating effect is evident in the contracted model, which also develops a clearer insight into the mechanisms involved. It is possible to include more general aggregation and fragmentation processes than the monomer−cluster interactions in the Becker−Döring scheme or to allow a more general mechanism for the breakoff of fragments from host vesicles; however, these additions greatly complicate the model and it is not apparent that they would result in better agreement with experiment. Future modeling challenges are expected to arise from the results of increasingly inventive experiments which are currently being performed.

Acknowledgment. Colin Bolton is supported by an EPSRC studentship. We thank P. L. Luisi for helpful conversations and permission to use Figure 1.

A. Appendix: Asymptotic Analysis: For Pure Monomeric Initial Data, $x_2^{(0)} = x_3^{(0)} = 0$

For completeness we include the time scale analysis for the case where initial data are given by $x_2^{(0)} = x_3^{(0)} = 0$, which differs from the case where the initial conditions are $\mathcal{O}(\epsilon)$ but the expressions for the critical times derived earlier are still valid. The differences include additional fast time scales at the start of the process.

A.1. Case $\lambda_3 + 1 < \lambda_2$. There are three relevant time scales: initially, the system passes through a very fast time scale with the scalings where x_2 and x_3 remain very small, at least an order of magnitude smaller than ϵ, namely

$$x_2 = \epsilon^{\lambda_2 - \lambda_3} y_2 \quad x_3 = \epsilon^{\lambda_2 - \lambda_3} y_3 \quad t = \epsilon^{-\lambda_3} t_1 \qquad \text{(A.1)}$$

where y_2 and y_3 are given by

$$y_2 = -\frac{\rho^{\lambda_2+1}}{\beta_3 + \rho^{\lambda_3}} e^{-(\beta_3+\rho^{\lambda_3})t_1} + \frac{\rho^{\lambda_2+1}}{\beta_3 + \rho^{\lambda_3}} - \frac{\beta_3 \rho^{\lambda_2+1}}{(\beta_3 + \rho^{\lambda_3})^2}[1 - e^{-(\beta_3+\rho^{\lambda_3})t_1}] + \frac{\beta_3 \rho^{\lambda_2+1} t_1}{\beta_3 + \rho^{\lambda_3}} \qquad \text{(A.2)}$$

$$y_3 = -\frac{\rho^{\lambda_3}\rho^{\lambda_2+1}}{(\beta_3 + \rho^{\lambda_3})^2}[1 - e^{-(\beta_3+\rho^{\lambda_3})t_1}] + \frac{\rho^{\lambda_3}\rho^{\lambda_2+1} t_1}{\beta_3 + \rho^{\lambda_3}} \qquad \text{(A.3)}$$

This scaling ceases to be valid due to y_2 and y_3 growing linearly

with t_1 as $t_1 \rightarrow \infty$, and we then enter the second time scale. New terms enter the leading order balance when $t = \mathcal{O}(\epsilon^{1-\lambda_2})$, and thus the second time scale spans a very long time, as can be seen by the scalings

$$x_2 = \epsilon z_2 \qquad x_3 = \epsilon z_3 \qquad t = \epsilon^{1-\lambda_2} t_2 \qquad \text{(A.4)}$$

Throughout this time scale x_2 and x_3 are in a local equilibrium with each other because the aggregation of monomers to x_2 is a slow process when compared to the exchange of mass between x_2 and x_3. We find that both x_2, $x_3 \rightarrow \infty$ at a critical time, t_{2c}, signaling the end of this time scale. Explicitly

$$z_2 = \frac{(\rho^{\lambda_3} + \beta_3)^{1/(\lambda_2-1)}\beta_3}{\rho^{(\lambda_2+1)/(\lambda_2-1)}(\alpha_{1,2}\beta_3 + \alpha_{1,3}\rho^{\lambda_3})^{\lambda_2/(\lambda_2-1)}(\lambda_2 - 1)^{1/(\lambda_2-1)}} \frac{1}{(t_{2c} - t_2)^{1/(\lambda_2-1)}} - \frac{\beta_3}{\alpha_{1,2}\beta_3 + \alpha_{1,3}\rho^{\lambda_3}} \qquad \text{(A.5)}$$

$$z_3 = \frac{(\rho^{\lambda_3} + \beta_3)^{\lambda_2/(\lambda_2-1)}}{\rho^{(\lambda_2+1)/(\lambda_2-1)}(\alpha_{1,2}\beta_3 + \alpha_{1,3}\rho^{\lambda_3})^{\lambda_2/(\lambda_2-1)}(\lambda_2 - 1)^{1/(\lambda_2-1)}} \frac{1}{(t_{2c} - t_2)^{1/(\lambda_2-1)}} - \frac{\rho^{\lambda_3} + \beta_3}{\alpha_{1,2}\beta_3 + \alpha_{1,3}\rho^{\lambda_3}} \qquad \text{(A.6)}$$

As x_2 and x_3 approach $\mathcal{O}(1)$, time scale three is entered, where now an appreciable number of monomers have been depleted and further aggregation is dominated by the catalytic effect. It only remains for the system to tend to its final equilibrium state, with the relevant scalings being $t = t_3 + \epsilon^{1-\lambda_2} t_{2c}$, $x_2 = z_2$, and $x_3 = z_3$.

A.2. Case $\lambda_2 < \lambda_3 + 1$. We note that because $\lambda_2 < \lambda_3 + 1$ we are investigating a system where x_2 represents a much smaller range of cluster sizes than x_3 and so we expect the dynamics of x_2 to be more closely related to that of the monomers. With initial conditions $x_2^{(0)} = x_3^{(0)} = 0$ we identify five asymptotic time scales. We first enter a long time scale where x_2 is $\mathcal{O}(\epsilon)$, but the concentration x_3 is much smaller, $\mathcal{O}(\epsilon^{\lambda_3-\lambda_2+2})$, and so we use the scaling

$$x_2 = \epsilon y_2 \quad x_3 = \epsilon^{\lambda_3-\lambda_2+2} y_3 \quad t = \epsilon^{1-\lambda_2} t_1 \qquad \text{(A.7)}$$

As x_2 increases the catalytic effect promotes the growth of x_2 and at the end of the first time scale we see a characteristic singularity in x_2 that signals the need to start the next time scale; solving for y_2 and y_3 yields

$$y_2 = \frac{1}{\alpha_{1,2}(1 - \alpha_{1,2}(\lambda_2 - 1)\rho^{\lambda_2+1} t_1)^{1/(\lambda_2-1)}} - \frac{1}{\alpha_{1,2}} \qquad \text{(A.8)}$$

$$y_3 = \frac{\rho^{\lambda_3}}{{\alpha_{1,2}}^2(\lambda_2 - 2)\rho^{\lambda_2+1}} - \frac{\rho^{\lambda_3}[1 - (\lambda_2 - 1)\rho^{\lambda_2+1}\alpha_{1,2}t_1]^{(\lambda_2-2)/(\lambda_2-1)}}{{\alpha_{1,2}}^2\rho^{\lambda_2+1}(\lambda_2 - 2)} - \frac{\rho^{\lambda_3} t_1}{\alpha_{1,2}} \qquad \text{(A.9)}$$

In the second time scale x_2 has grown to $\mathcal{O}(1)$, but x_3 remains much smaller and the time scale is relatively very fast, that is

$$x_2 = \mathcal{O}(1) \quad x_3 = \epsilon^{\lambda_3-\lambda_2+2} z_3 \quad t = t_2 + \epsilon^{1-\lambda_2} t_{1c} \qquad \text{(A.10)}$$

This time scale is relatively fast, and the x_3 coordinate appears constant and x_2 equilibrates with the monomer concentration; that is, $x_2 \rightarrow x_{2con}$ where x_{2con} satisfies (3.35) and

$$z_3(t_2) = \frac{\rho^{\lambda_3}}{{\alpha_{1,2}}^2(\lambda_2 - 1)(\lambda_2 - 2)\rho^{\lambda_2+1}} \qquad \text{(A.11)}$$

We must now endure another long time scale before x_3 reaches $\mathcal{O}(1)$ values, and so we rescale according to

$$x_2 = p_2 \quad x_3 = \epsilon^{\lambda_3-\lambda_2+2} p_3 \quad t = \epsilon^{2-\lambda_2} t_3 + \epsilon^{1-\lambda_2} t_{1c} \qquad \text{(A.12)}$$

The x_2 concentration remains constant (equal to x_{2con}), but x_3 grows linearly throughout this time scale, that is

$$p_3 = x_{2con}(\rho - \lambda_2\Lambda_2 x_{2con})^{\lambda_3} t_3 + \frac{\rho^{\lambda_3}}{{\alpha_{1,2}}^2(\lambda_2 - 1)(\lambda_2 - 2)\rho^{\lambda_2+1}} \qquad \text{(A.13)}$$

and eventually the time scale ends when x_3 reaches $\mathcal{O}(\epsilon)$, which occurs when $t_3 \sim \mathcal{O}(\epsilon^{\lambda_2-\lambda_2-1})$. Hence the fourth time scale is given by

$$x_2 = q_2 \quad x_3 = \epsilon q_3 \quad t = \epsilon^{1-\lambda_3} t_4 + \epsilon^{1-\lambda_2} t_{1c} \qquad \text{(A.14)}$$

Over this long time scale x_2 does not change; however, x_3 increases and approaches a singularity as it reaches even larger values and we find

$$q_3 = \frac{1}{\alpha_{2,3}[\alpha_{2,3}(\lambda_3 - 1)x_{2con}(\rho - \lambda_2\Lambda_2 x_{2con})^{\lambda_3}(t_{3c} - t_4)]^{1/(\lambda_3-1)}} - \frac{1}{\alpha_{2,3}} \qquad \text{(A.15)}$$

where we have denoted the constant of integration as t_{3c} to indicate that it has exactly the same form as that given earlier (3.40). Once x_3 reaches an $\mathcal{O}(1)$ quantity then we enter the final, fast, time scale with scalings

$$x_2 = r_2 \quad x_3 = r_3 \quad t = t_5 + \epsilon^{1-\lambda_3} t_{3c} + \epsilon^{1-\lambda_2} t_{1c} \qquad \text{(A.16)}$$

Over this fast time scale the system tends to the global equilibrium state.

References and Notes

(1) Oró, J.; Miller, S. L.; Lazcano, A. *Annu. Rev. Earth Planet. Sci.* **1990**, *18*, 317.
(2) Bolton, C. D.; Wattis, J. A. D. *J. Phys. Chem. B* **2003**, *107*, 7126.
(3) Becker, R.; Döring, W. *Ann. Phys.* **1935**, *24*, 719.
(4) Walde, P.; Wick, R.; Fresta, M.; Mangone, A.; Luisi, P. L. *J. Am. Chem. Soc.* **1994**, *116*, 11649
(5) Blöchliger, E.; Blocher, M.; Walde, P.; Luisi, P. L. *J. Phys. Chem. B* **1998**, *102*, 10383.
(6) Mavelli, F.; Luisi, P. L. *J. Phys. Chem.* **1996**, *100*, 16600.
(7) Coveney, P. V.; Wattis, J. A. D. *J. Chem. Soc., Faraday Trans.* **1998**, *94*, 233.
(8) Lonchin, S.; Luisi, P. L.; Walde, P.; Robinson, B. H. *J. Phys. Chem. B* **1999**, *103*, 10910.
(9) Berclaz, N.; Blöchliger, E.; Müler, M.; Luisi, P. L. *J. Phys. Chem. B* **2001**, *105*, 1065.
(10) Berclaz, N.; Müler, M.; Walde, P.; Luisi, P. L. *J. Phys. Chem. B* **2001**, *105*, 1056.
(11) Penrose, O.; Lebowitz, J. L. *Studies in Statistical Mechanics VII: Fluctuation Phenomena*; North-Holland, Amsterdam, 1976.
(12) Coveney, P. V.; Wattis, J. A. D. *Proc. R. Soc. London A* **1996**, *452*, 2079.

(13) Bolton, C. D.; Wattis, J. A. D. Generalisd coarse-grained Becker−Döring equations. *J. Phys. A; Math. Gen.* **2003**, *36*, 7859.
(14) Wattis, J. A. D.; Coveney, P. V. *J. Chem. Phys.* **1997**, *106*, 9122.
(15) Wattis, J. A. D.; Coveney, P. V. *J. Phys. A: Math. Gen.* **2001**, *34*, 8679
(16) Wattis, J. A. D.; Coveney, P. V. *J. Phys. A: Math. Gen.* **2001**, *34*, 8697.
(17) Hinch, E. J. *Perturbation methods*; Cambridge University Press: Cambridge, U.K., 1991.
(18) Glendinning, P. *Stability, instability and chaos: an introduction to the theory of nonlinear differential equations*; Cambridge University Press: Cambridge, U.K., 1994.
(19) Murray, J. D. *Mathematical Biology*; Springer: Berlin, 1993.